Human and natural influences on the changing thermal structure of the atmosphere

Benjamin D. Santer[a,1], Jeffrey F. Painter[a], Céline Bonfils[a], Carl A. Mears[b], Susan Solomon[c], Tom M. L. Wigley[d,e], Peter J. Gleckler[a], Gavin A. Schmidt[f], Charles Doutriaux[a], Nathan P. Gillett[g], Karl E. Taylor[a], Peter W. Thorne[h], and Frank J. Wentz[b]

[a]Program for Climate Model Diagnosis and Intercomparison, Lawrence Livermore National Laboratory, Livermore, CA 94550; [b]Remote Sensing Systems, Santa Rosa, CA 95401; [c]Earth, Atmospheric, and Planetary Sciences, Massachusetts Institute of Technology, Cambridge, MA 02139; [d]National Center for Atmospheric Research, Boulder, CO 80307; [e]School of Earth and Environmental Sciences, University of Adelaide, Adelaide, SA 5005, Australia; [f]National Aeronautics and Space Administration/Goddard Institute for Space Studies, New York, NY 10025; [g]Canadian Centre for Climate Modelling and Analysis, Environment Canada, Victoria, BC, Canada V8W 2Y2; and [h]Nansen Environmental and Remote Sensing Center, N-5006 Bergen, Norway

Since the late 1970s, satellite-based instruments have monitored global changes in atmospheric temperature. These measurements reveal multidecadal tropospheric warming and stratospheric cooling, punctuated by short-term volcanic signals of reverse sign. Similar long- and short-term temperature signals occur in model simulations driven by human-caused changes in atmospheric composition and natural variations in volcanic aerosols. Most previous comparisons of modeled and observed atmospheric temperature changes have used results from individual models and individual observational records. In contrast, we rely on a large multimodel archive and multiple observational datasets. We show that a human-caused latitude/altitude pattern of atmospheric temperature change can be identified with high statistical confidence in satellite data. Results are robust to current uncertainties in models and observations. Virtually all previous research in this area has attempted to discriminate an anthropogenic signal from internal variability. Here, we present evidence that a human-caused signal can also be identified relative to the larger "total" natural variability arising from sources internal to the climate system, solar irradiance changes, and volcanic forcing. Consistent signal identification occurs because both internal and total natural variability (as simulated by state-of-the-art models) cannot produce sustained global-scale tropospheric warming and stratospheric cooling. Our results provide clear evidence for a discernible human influence on the thermal structure of the atmosphere.

climate change detection | climate modeling

Global changes in the physical climate system are driven by both internal variability and external influences (1, 2). Internal variability is generated by complex interactions of the coupled atmosphere–ocean system, such as the well-known El Niño/Southern Oscillation. External influences include human-caused changes in well-mixed greenhouse gases, stratospheric ozone, and other radiative forcing agents, as well as natural fluctuations in solar irradiance and volcanic aerosols. Each of these external influences has a unique "fingerprint" in the detailed latitude/altitude pattern of atmospheric temperature change (3–8). The use of such fingerprint information has proved particularly useful in separating human, solar, and volcanic influences on climate, and in discriminating between externally forced signals and internal variability (3–7).

We have two main scientific objectives. The first is to consider whether a human-caused fingerprint can be identified against the "total" natural variability (V_{TOT}) arising from the combined effects of internal oscillatory behavior (V_{INT}), solar irradiance changes, and fluctuations in atmospheric loadings of volcanic aerosols. To date, only one signal detection study (involving hemispheric-scale surface temperature changes) has relied on V_{TOT} information (9). All other pattern-based fingerprint studies have tested against V_{INT} (2, 4–7, 10, 11). When fingerprint investigations use information from simulations with natural external forcing, it is typically for the purpose of ascertaining whether

model-predicted solar and volcanic signals are detectable in observational climate records, and whether the amplitude of the model signals is consistent with observed estimates of signal strength (7, 12, 13).

We are addressing a different statistical question here. We seek to determine whether observed changes in the large-scale thermal structure of the atmosphere are truly unusual relative to the best current estimates of the total natural variability of the climate system. The significance testing framework applied here is highly conservative. Our V_{TOT} estimates incorporate variability information from 850 AD to 2005, and sample substantially larger naturally forced changes in volcanic aerosol loadings and solar irradiance than have been observed over the satellite era.

Our second objective is to examine the sensitivity of fingerprint results to current uncertainties in models and observations. With one exception (11), previous fingerprint studies of changes in the vertical structure of atmospheric temperature have used information from individual models. An additional concern is that observational uncertainty is rarely considered in such work (3–7). These limitations have raised questions regarding the reliability of fingerprint-based findings of a discernible human influence on climate (14).

Model and Observational Temperature Data

The model output analyzed here is from phase 5 of the Coupled Model Intercomparison Project (CMIP-5) (15). We use atmospheric

Significance

Observational satellite data and the model-predicted response to human influence have a common latitude/altitude pattern of atmospheric temperature change. The key features of this pattern are global-scale tropospheric warming and stratospheric cooling over the 34-y satellite temperature record. We show that current climate models are highly unlikely to produce this distinctive signal pattern by internal variability alone, or in response to naturally forced changes in solar output and volcanic aerosol loadings. We detect a "human influence" signal in all cases, even if we test against natural variability estimates with much larger fluctuations in solar and volcanic influences than those observed since 1979. These results highlight the very unusual nature of observed changes in atmospheric temperature.

temperature changes from simulations with estimated historical changes in these factors: (*i*) combined human and natural external forcings (ALL); (*ii*) anthropogenic forcings only (ANT); (*iii*) combined solar and volcanic forcing only (NAT); (*iv*) solar forcing only (SOL); and (*v*) volcanic forcing only (VOL). We also analyze integrations with the following: (*vi*) estimated changes in solar and volcanic forcing over the past 1,000 y (P1000); (*vii*) no changes in external influences (CTL); and (*viii*) 21st century changes in greenhouse gases and anthropogenic aerosols (16) specified according to Representative Concentration Pathway 8.5 (RCP8.5).

We compare simulation output with observed atmospheric temperature changes inferred from satellite-based Microwave Sounding Units (MSUs). Our focus is on zonally averaged temperature changes for three broad layers of the atmosphere: the lower stratosphere (TLS), the mid- to upper troposphere (TMT), and the lower troposphere (TLT) (1). We use observational MSU information from two different groups: Remote Sensing Systems (RSS) (17) and the University of Alabama at Huntsville (UAH) (18). An important aspect of our fingerprint study is its use of additional estimates of observational uncertainty provided by the RSS group (17) (*SI Appendix*).

Two processing choices facilitate the comparison of models and observations. First, we calculate synthetic MSU temperatures from CMIP-5 simulations, so that modeled and observed layer-averaged temperatures are vertically weighted in a similar way (10). Second, we splice together temperature information from the ALL and RCP8.5 simulations. The latter are initiated from the end of the ALL simulations, which was generally in December 2005 (*SI Appendix*). Splicing makes it possible to compare modeled and observed temperature changes over the full observed satellite record. We refer to these spliced simulations as "ALL+8.5." (The ANT, NAT, VOL, and SOL integrations also end in December 2005. Unlike the ALL simulation, they cannot be spliced with RCP8.5 results without introducing a discontinuity in forcing.)

Global-Mean Temperature Changes

Fig. 1 shows the multimodel average changes in global-mean atmospheric temperature in the NAT and ALL+8.5 simulations. In both types of numerical experiment, the stratosphere warms and the troposphere cools after major volcanic eruptions (1, 4–8, 19, 20). The abrupt TLS warming signals (Fig. 1*A*) are due to the absorption of incoming solar radiation and outgoing long-wave radiation by volcanic aerosols injected into the stratosphere (21). Stratospheric volcanic aerosols also reduce the clear-sky solar radiation received at Earth's surface, leading to surface and tropospheric cooling. Because of the large thermal inertia of the oceanic mixed layer, the recovery of tropospheric temperature from volcanically induced cooling can take up to a decade (Fig. 1 *B* and *C*). The removal of volcanic aerosols and the recovery of lower stratospheric temperature is more rapid (~2 y).

The ALL+8.5 simulations exhibit sustained cooling of the lower stratosphere and warming of the troposphere over the past 60 y (Fig. 1). The decrease in TLS is primarily a response to human-caused stratospheric ozone depletion, with a smaller contribution from anthropogenic changes in other greenhouse gases (GHGs) (19, 22, 23). Tropospheric warming is mainly driven by anthropogenic GHG increases (1, 2, 8, 23, 24). In contrast, the NAT runs do not produce large, multidecadal temperature changes (Fig. 1 and *SI Appendix*, Figs. S1 and S2).

After removing the climatological seasonal cycle, lower stratospheric temperature anomalies exhibit a large (post-1970) residual seasonal cycle in the ALL+8.5 simulation, but not in the NAT integration (Fig. 1*A*). This residual seasonality arises because of the pronounced impact of stratospheric ozone depletion on the seasonal cycle of TLS, particularly at high latitudes in the Southern Hemisphere (25, 26) (*SI Appendix*, Fig. S3).

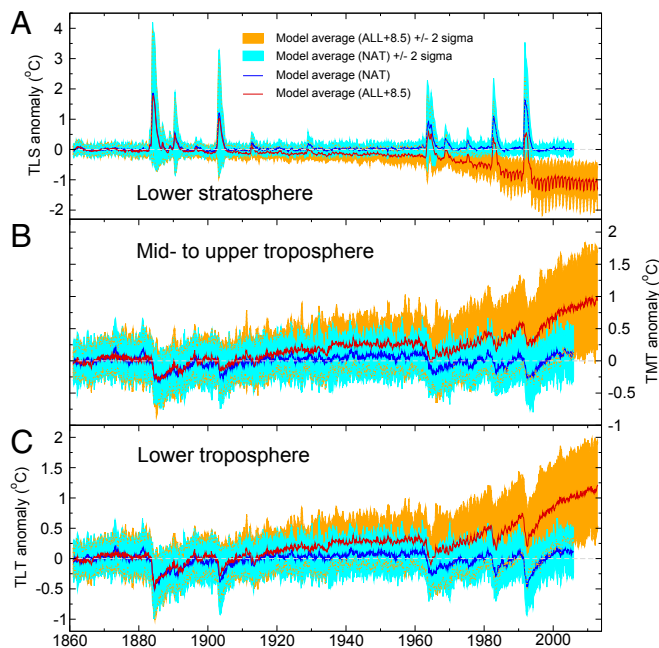**Atmospheric Temperature Changes in CMIP-5 Simulations**

Model average (ALL+8.5) +/- 2 sigma
Model average (NAT) +/- 2 sigma
Model average (NAT)
Model average (ALL+8.5)

A Lower stratosphere
B Mid- to upper troposphere
C Lower troposphere

Fig. 1. Time series of simulated monthly mean near-global anomalies in the temperature of the lower stratosphere (TLS), the mid- to upper troposphere (TMT), and the lower troposphere (TLT) (*A–C*). Model results are from spliced historical/RCP8.5 simulations with combined anthropogenic and natural external forcing (ALL+8.5) and from simulations with natural external forcing only (NAT). The bold lines denote the ALL+8.5 and NAT multimodel averages, calculated with 20 and 16 CMIP-5 models (respectively). Temperatures are averaged over 82.5°N–82.5°S for TLS and TMT, and over 82.5°N–70°S for TLT. Anomalies are defined with respect to climatological monthly means over 1861–1870. The shaded envelopes are the multimodel averages $\pm 2 \times s(t)$, where $s(t)$ is the "between model" SD of the 20 (ALL+8.5) and 16 (NAT) ensemble-mean anomaly time series. To aid visual discrimination of the overlapping ALL+8.5 and NAT envelopes, the boundaries of the ALL+8.5 envelope are indicated by dotted orange lines.

Latitude/Altitude Patterns of Temperature Change

Fig. 2 shows the vertical structure of zonal-mean atmospheric temperature trends in the observations and the ALL+8.5, ANT, NAT, VOL, and SOL simulations. Because we perform our subsequent fingerprint analysis in "MSU space," with only three atmospheric layers (TLS, TMT, and TLT), we use the same MSU space here for visual display of temperature trends. This provides a vertically smoothed picture of temperature changes over the satellite era, while still preserving the principal large-scale features of externally forced signals. [The contouring algorithm used to generate Fig. 2 interpolates temperature information between vertical layers, and between 5° latitude bands (see legend of Fig. 2).]

The ALL+8.5 and ANT multimodel averages (Fig. 2 *A* and *D*) and the observations (Fig. 2 *H* and *I*) are characterized by similar patterns of large-scale tropospheric warming and lower stratospheric cooling. In the ALL+8.5 simulations, the most pronounced intermodel differences in temperature trends are in the vicinity of the Antarctic ozone hole (Fig. 2*B* and *SI Appendix*, Fig. S4), where internal variability is large (10), and there are appreciable intermodel differences in historical ozone forcing (27).

If we use the ratio R_1 as a measure of the size of the multimodel average ALL+8.5 trend relative to the intermodel SD of ALL+8.5 temperature trends, this metric exceeds two over substantial portions of the troposphere and lower stratosphere (Fig. 2*C*). The R_1 results demonstrate that the ALL+8.5 pattern of tropospheric warming and stratospheric cooling is robust to current uncertainties in external forcings and model temperature responses.

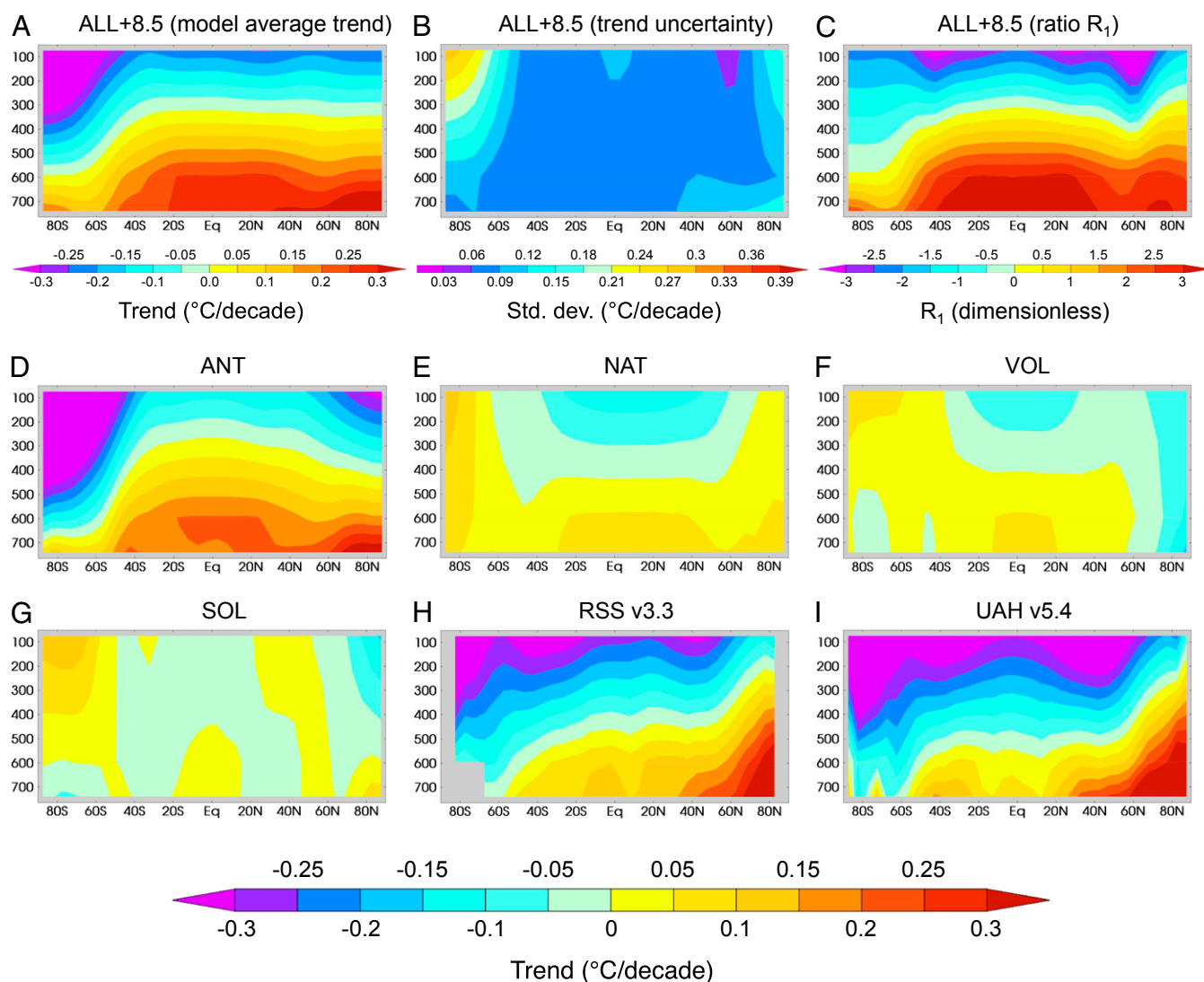# Zonal-Mean Atmospheric Temperature Trends in CMIP-5 Models and Observations

Fig. 2. Zonal-mean atmospheric temperature trends in CMIP-5 models (*A* and *D–G*) and observations (*H* and *I*). Trends were calculated after first regridding model and observational TLS, TMT, and TLT anomaly data to a 5°×5° latitude/longitude grid, and then computing zonal averages. Results are plotted in "MSU space," at the approximate peaks of the TLS, TMT, and TLT global-mean MSU weighting functions (74, 595, and 740 hPa, respectively). Trends in the RSS and UAH observations and the ALL+8.5 simulations are for the 408 months from January 1979 to December 2012. For the shorter ANT, NAT, VOL, and SOL simulations, trends are over January 1979 to December 2005. The ALL+8.5, ANT, NAT, VOL, and SOL trends are multimodel averages, computed with 20, 8, 16, 2, and 3 models (respectively). *B* shows a simple measure of model uncertainty in the ALL+8.5 trends: $s(x,h)$, the intermodel SD of the 20 individual ensemble-mean trends. The ratio R_1 in *C* is the ALL+8.5 multimodel average trend in *A*, $\bar{\bar{b}}(x,h)$, divided by $s(x,h)$ in *B*.

Anthropogenic forcing makes the largest contribution to the ALL+8.5 temperature-change pattern (Fig. 2 *A* and *D–G*). The NAT contribution is relatively small, but augments the anthropogenic signal. Over 1979–2005, the NAT contribution is dominated by volcanic effects, which generate a slight warming trend in the troposphere and a small cooling trend in the stratosphere (*SI Appendix*, Fig. S5). Because there is little or no trend in solar irradiance over the satellite era, the simulated solar signal is weak.

It is difficult to make more rigorous quantitative comparisons of the temperature changes in the ALL+8.5, ANT, NAT, SOL, and VOL simulations. This difficulty arises because of (*i*) "between experiment" differences in the number of models and realizations available for estimating multimodel averages (*SI Appendix*); and (*ii*) "between model" differences in external forcings (27) and climate sensitivity (28). The information provided in Fig. 2, however, represents our current best multimodel estimate of the

patterns and relative sizes of anthropogenically and naturally forced atmospheric temperature changes over the satellite era.

Leading Signal and Noise Patterns

We use a standard fingerprint method (29) to compare model-predicted vertical patterns of zonal-mean atmospheric temperature change with satellite observations (*SI Appendix*). The searched-for fingerprint is the climate-change signal in response to a set of external forcings. Here, the fingerprint is defined as the first empirical orthogonal function (EOF) of $\bar{\bar{S}}(x,h,t)$, the multimodel average of zonal-mean synthetic MSU temperature changes in the ANT or ALL+8.5 simulations. [The double overbar in $\bar{\bar{S}}(x,h,t)$ indicates two averaging steps: an average over ANT or ALL+8.5 realizations of an individual model (if multiple realizations are available) and an average over models.]

As in the observations (Fig. 2 *H* and *I*), both the ANT and ALL+8.5 fingerprints show spatially coherent warming of the troposphere and cooling of the lower stratosphere (Fig. 3 *A* and *B*). The similarity of the ANT and ALL+8.5 fingerprints arises because model trends in atmospheric temperature over the past 30–60 y are primarily driven by anthropogenic influences, with only a small contribution from solar and volcanic forcing (Figs. 1 and 2).

Before presenting the results of our fingerprint analysis, we first examine the major modes of internal and total natural variability (Fig. 3 *C–K*). These are characterized by the leading EOFs calculated from the CTL, NAT, and P1000 simulations (*SI Appendix*). In the first EOF of the CTL simulations, temperature changes in the tropics and extratropics are negatively correlated (Fig. 3*C*). The leading mode in the NAT and P1000 simulations used to estimate V_{TOT} (Fig. 3 *F* and *I*) captures both the stratospheric warming and tropospheric cooling in response to large volcanic eruptions and part of the internal variability manifest in CTL EOF 1 (Fig. 3*C*). The natural variability modes in Fig. 3 *C–K*

lack the pattern of global-scale tropospheric warming and stratospheric cooling that is evident in the observations (Fig. 2 *H* and *I*) and the ANT and ALL+8.5 fingerprints (Fig. 3 *A* and *B*).

Fingerprint Results

We consider next the detectability of the ANT fingerprint. If the amplitude of the fingerprint pattern $F(x,h)$ is increasing in $O(x,h,t)$, the time-varying observations, there will be a positive trend in $c\{F,O\}(t)$, the covariance statistic that measures the spatial similarity between $F(x,h)$ and $O(x,h,t)$ (*SI Appendix*). [The indices x, h, and t are (respectively) over the total number of latitude bands, atmospheric layers, and time (in years).] These "signal" trends," $b(L)$, are a function of the analysis period L, which spans lengths of 10–34 y (i.e., from 1979–1988 to 1979–2012).

As L increases, the spatial similarity between $O(x,h,t)$ and the ANT fingerprint decreases initially due to the stratospheric warming and tropospheric cooling caused by the 1991 Pinatubo eruption (Fig. 4*A*). This reduces the magnitude of $b(L)$ values.

Leading Signal and Natural Variability Modes in CMIP-5 Models

Fig. 3. Leading signal and natural variability modes for the vertical structure of atmospheric temperature change in CMIP-5 simulations. All signal and natural variability modes were calculated after first transforming annual-mean synthetic TLS, TMT, and TLT data to a common 5° × 5° latitude/longitude grid, and then computing zonal averages. The leading signal modes are the first EOFs of the multimodel atmospheric temperature changes in the ANT and ALL+8.5 simulations (*A* and *B*, respectively). Multimodel averages were calculated over 1861–2012 for the ALL+8.5 case, and over 1861–2005 for the shorter ANT simulations, using results from 20 ALL+8.5 models and 8 ANT models. The leading natural variability modes are EOFs 1, 2, and 3 of the 20 concatenated preindustrial control runs (CTL; *C–E*), the 16 concatenated simulations with estimates of historical changes in solar and volcanic forcing over 1850–2005 (NAT; *F–H*), and the 6 concatenated integrations with natural external forcing over 850–1700 (P1000; *I–K*). The percentage variance explained by each mode is given in parentheses. See *SI Appendix* for further analysis details.

During the recovery phase after Pinatubo, signal trends increase until $L = 20$ years. Subsequently, following the large tropospheric warming caused by the 1997/1998 El Niño, the amplitude of $b(L)$ gradually decreases. This decrease is due to changes in observed rates of stratospheric cooling and troposphere warming (10, 30).

The crux of the fingerprint identification problem is to assess whether these signal trends are statistically significant. We use signal-to-noise (S/N) ratios to make this determination. To estimate the denominator of the S/N ratio, we require "null" (no signal) distributions for trends of length L years. Conventionally, these distributions are obtained using internal variability information from many L-year segments of CTL simulations. Here, we also consider the additional variability arising from solar and volcanic forcing, which we estimate using both the NAT integrations and the longer P1000 runs. This gives us three different sets of natural variability estimates and S/N ratios (Fig. 4 *B* and *C*; green, blue, and red curves).

We obtain "no signal" distributions by comparing $F(x,h)$ with $N(x,h,t)$, the temperature changes from the concatenated CTL, NAT, or P1000 integrations. This yields long time series of the pattern similarity statistic $c\{F,N\}(t)$, from which the null distributions can be calculated for varying trend lengths. These distributions have means close to zero and standard deviations $s(L)$ that decrease by a factor of roughly 5 as L increases from 10 to 34 y (Fig. 4*B*).

The S/N ratio that we use for assessing the statistical significance of signal trends is simply given by $b(L)/s(L)$ (Fig. 4*C*). [For $L = 10$, therefore, $b(L)$ is calculated over 1979–1988, and $s(L)$ is computed from the distribution of nonoverlapping 10-y trends in $c\{F,N\}(t)$.] S/N ratios generally increase with longer analysis periods, primarily because of the decrease in $s(L)$ with larger values of L. With CTL noise, S/N ratios for signal trends computed over 1979–2012 are invariably significant at the 1% level or better, and range from 8.4 to 10.7, depending on the choice of observational dataset.

Consider next the S/N results for tests against V_{TOT}. The NAT simulations provide estimates of how atmospheric temperature might have evolved in the absence of human intervention, but in the presence of stochastic temperature changes arising from internal variability and deterministic changes caused by solar and volcanic forcing. One possible significance testing strategy is to restrict our estimate of V_{TOT} to the period of overlap between the NAT runs and the satellite data sets (1979–2005). This strategy has two disadvantages: (*i*) we have only 16 NAT models with samples of naturally forced temperature change over 1979–2005; and (*ii*) each of these samples includes only two major volcanic eruptions (El Chichón and Pinatubo).

Here, we estimate V_{TOT} over 1861–2005, and thus do not require that the simulated and observed evolution of volcanic forcing is identical. By using this longer period, we include the effects of four additional major eruptions in the presatellite era (Krakatau in 1883, Soufrière/Pelée/Santa Maria in 1902, Novarupta in 1912, and Agung in 1963) and obtain many more samples of the temperature response to volcanic forcing. This increase in sample size is advantageous in assessing the likelihood of obtaining the observed signal trends by total natural variability alone.

As expected, trends computed from the NAT simulations are generally larger than those obtained from the CTL runs (Fig. 4*B*). This holds for all timescales examined here. Despite the increase in the size of the denominator, S/N ratios remain highly significant for signal trends calculated over the full satellite record, ranging from 3.7 to 4.8 (Fig. 4*C*). It is unlikely that these values are spuriously inflated by a systematic underestimate of total natural variability in the CMIP-5 models analyzed here (10).

Although there are large uncertainties in the solar and volcanic forcings used in the six P1000 runs (31), these simulations provide our best current estimates of the magnitude and patterns of naturally forced atmospheric temperature change over the period from 850 to 1849 (*SI Appendix*, Fig. S6). As in the case of the NAT simulations, we use P1000 V_{TOT} estimates to determine whether an anthropogenic fingerprint can be identified relative to

Signal Trends, Noise Trends, and S/N Ratios

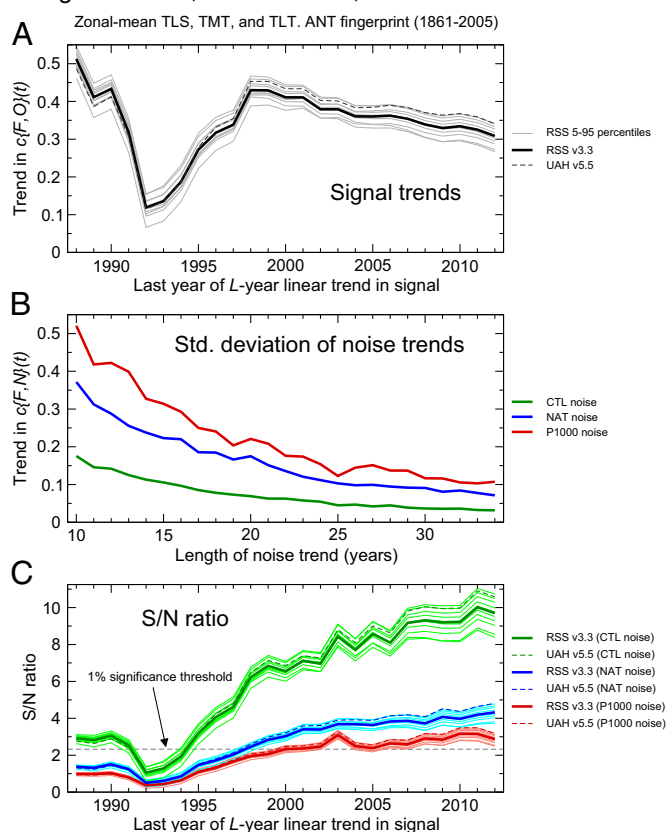Zonal-mean TLS, TMT, and TLT. ANT fingerprint (1861-2005)

Fig. 4. Results from the S/N analysis of simulated and observed changes in zonal-mean TLS, TMT, and TLT. Signal time series provide information on the similarity between the time-invariant ANT fingerprint pattern (Fig. 3*A*) and the time-varying observed patterns of zonal-mean atmospheric temperature change. Values of $b(L)$, the L-year trends in these signal time series, are plotted in *A*. Noise time series indicate the level of similarity between the ANT fingerprint and the CTL, NAT, and P1000 estimates of variability. *B* shows $s(L)$, the SD of the distribution of nonoverlapping L-year trends in the CTL, NAT, and P1000 noise time series. The S/N ratio between $b(L)$ and $s(L)$ is given in *C*. The thin solid lines in *C* are the S/N ratios for signal trends obtained with the RSS 5–95 percentiles. The nominal 1% significance level assumes a Gaussian distribution of noise trends. The ANT fingerprint was calculated using the multimodel average zonal-mean changes in atmospheric temperature over 1861–2005 (*SI Appendix*). Signal and noise trends in *A* and *B* have units of c{F,O}/decade and c{F,N}/decade, respectively.

total natural variability levels that are substantially larger than those actually sampled over the satellite era.

In addition to solar and volcanic forcing, the P1000 simulations include anthropogenic changes in GHGs and land use (31). To avoid appreciable anthropogenic contamination, V_{TOT} values were calculated using synthetic MSU temperatures for 850–1700 only. This period contains at least two massive volcanic eruptions—an unknown eruption in 1259, and Kuwae in 1452. Each event is estimated to have produced larger stratospheric sulfate aerosol loadings than those of any eruption during the NAT simulation period (32). This explains why the P1000 levels of total natural variability are consistently higher than those computed with NAT simulations (Fig. 4*B*). Even with these very large P1000 V_{TOT} values, we still obtain ubiquitous detection of an anthropogenic fingerprint in the observations, with S/N ratios ranging from 2.5 to 3.2 for 34-y trends (Fig. 4*C*).

Sensitivity Tests

We performed a number of additional sensitivity studies to explore the robustness of these results. The first involved use of the

ALL+8.5 rather than the ANT fingerprint. Because of the spatial similarity of these fingerprints, they yield similar S/N ratios (Fig. 4 and *SI Appendix*, Fig. S7). In a second test, we repeated the entire fingerprint analysis with zonal-mean changes in TLS and TLT only. Temperature changes have more favorable S/N characteristics in the lower stratosphere than in the troposphere (10), so removal of zonal-mean TMT changes substantially increases S/N ratios (*SI Appendix*, Fig. S8). In our third test, ALL +8.5 and ANT fingerprints were estimated over the satellite era only (rather than over the full period of these simulations). Use of a shorter period for fingerprint estimation still preserves the large-scale features of tropospheric warming and stratospheric cooling (Fig. 2 *A* and *D*), so fingerprint detection is insensitive to this analysis choice.

One area of concern is that, on average, the ALL+8.5 simulations underestimate the observed lower stratospheric cooling and overestimate tropospheric warming (compare Fig. 2*A* with Fig. 2 *H* and *I*). These differences must be due to some combination of errors in model forcings (27, 33–35), model response errors (36), residual observational inhomogeneities (17), and an unusual manifestation of natural internal variability in the observations (10, 30). Because of the bias in tropospheric warming, most individual models have S/N ratios that are larger than those obtained with observations (*SI Appendix*, Fig. S9).

Conclusions

Our analysis of the latest satellite datasets and model simulations reveals that a model-predicted anthropogenic fingerprint pattern is consistently identifiable, with high statistical confidence, in the changing thermal structure of the atmosphere. Multidecadal tropospheric warming and lower stratospheric cooling are the main features of this fingerprint. Tests against NAT and P1000 "total" natural variability (V_{TOT}) demonstrate that observed temperature changes are not simply a recovery from the El Chichón and Pinatubo events, and/or a response to variations in solar irradiance. The significance testing framework used here is highly conservative—the NAT and P1000 estimates of V_{TOT} include volcanic eruptions and solar irradiance changes much larger than those observed over the satellite era. Our results are robust to current uncertainties in models and observations, and underscore the dominant role human activities have played in recent climate change.

1. Karl TR, Hassol SJ, Miller CD, Murray WL, eds (2006) *Temperature Trends in the Lower Atmosphere: Steps for Understanding and Reconciling Differences. A Report by the U.S. Climate Change Science Program and the Subcommittee on Global Change Research* (National Oceanic and Atmospheric Administration, National Climatic Data Center, Asheville, NC).
2. Hegerl GC, et al. (2007) Understanding and attributing climate change. *Climate Change 2007: The Physical Science Basis. Contribution of Working Group I to the Fourth Assessment Report of the Intergovernmental Panel on Climate Change*, eds Solomon S, et al. (Cambridge Univ Press, Cambridge, UK).
3. Karoly DJ, et al. (1994) An example of fingerprint detection of greenhouse climate change. *Clim Dyn* 10:97–105.
4. Santer BD, et al. (1996) A search for human influences on the thermal structure of the atmosphere. *Nature* 382:39–46.
5. Vinnikov KYa, Robock A, Stouffer RJ, Manabe S (1996) Vertical patterns of free and forced climate variations. *Geophys Res Lett* 23:1801–1804.
6. Tett SFB, Mitchell JFB, Parker DE, Allen MR (1996) Human influence on the atmospheric vertical temperature structure: Detection and observations. *Science* 274(5290): 1170–1173.
7. Thorne PW, et al. (2002) Assessing the robustness of zonal mean climate change detection. *Geophys Res Lett* 29(19):1920, 10.1029/2002GL015717.
8. Hansen JE, et al. (2005) Efficacy of climate forcings. *J Geophys Res* 110:D18104, 10.1029/2005JD005776.
9. Hegerl GC, et al. (2007) Detection of human influence on a new, validated 1500-year temperature reconstruction. *J Clim* 20:650–666.
10. Santer BD, et al. (2013) Identifying human influences on atmospheric temperature. *Proc Natl Acad Sci USA* 110(1):26–33.
11. Lott FC, et al. (2013) Models versus radiosondes in the free atmosphere: A new detection and attribution analysis of temperature. *J Geophys Res* 118:2609–2619.
12. Tett SFB, et al. (2002) Estimation of natural and anthropogenic contributions to twentieth century temperature change. *J Geophys Res* 107:D16, 10.1029/2000JD000028.
13. Gillett NP, et al. (2011) Attribution of observed changes in stratospheric ozone and temperature. *Atmos Chem Phys* 11:599–609.
14. Curry JA, Webster PJ (2011) Climate science and the uncertainty monster. *Bull Am Meteorol Soc* 92(12):1667–1682.
15. Taylor KE, Stouffer RJ, Meehl GA (2012) An overview of CMIP5 and the experiment design. *Bull Am Meteorol Soc* 93(4):485–498.
16. Meinshausen M, et al. (2011) The RCP greenhouse gas concentrations and their extensions from 1765 to 2300. *Clim Change* 109(1-2):213–241, 10.1007/s10584-011-0156-z.
17. Mears C, Wentz FJ, Thorne P, Bernie D (2011) Assessing uncertainty in estimates of atmospheric temperature changes from MSU and AMSU using a Monte-Carlo technique. *J Geophys Res* 116:D08112, 10.1029/2010JD014954.
18. Christy JR, Norris WB, Spencer RW, Hnilo JJ (2007) Tropospheric temperature change since 1979 from tropical radiosonde and satellite measurements. *J Geophys Res* 112:D06102, 10.1029/2005JD006881.
19. Ramaswamy V, et al. (2006) Anthropogenic and natural influences in the evolution of lower stratospheric cooling. *Science* 311(5764):1138–1141.
20. Wigley TML, Ammann CM, Santer BD, Raper SCB (2005) The effect of climate sensitivity on the response to volcanic forcing. *J Geophys Res* 110:D09107, 10.1029/2004/JD005557.
21. Ramaswamy V, et al. (2001) Stratospheric temperature trends: Observations and model simulations. *Rev Geophys* 39:71–122.
22. Seidel DJ, Gillett NP, Lanzante JR, Shine KP (2011) Stratospheric temperature trends: Our evolving understanding. *Wiley Interdiscip Rev* 2:592–616, 10.1002/wcc.125.
23. Santer BD, et al. (2003) Contributions of anthropogenic and natural forcing to recent tropopause height changes. *Science* 301(5632):479–483.
24. Thorne PW, Lanzante JR, Peterson TC, Seidel DJ, Shine KP (2011) Tropospheric temperature trends: History of an ongoing controversy. *Wiley Interdiscip Rev* 2:66–88, 10.1002/wcc.80.
25. Thompson DWJ, et al. (2011) Signatures of the Antarctic ozone hole in Southern Hemisphere surface climate change. *Nat Geosci* 4:741–749.
26. Gillett NP, Thompson DWJ (2003) Simulation of recent southern hemisphere climate change. *Science* 302(5643):273–275.
27. Eyring V, et al. (2013) Long-term changes in tropospheric and stratospheric ozone and associated climate impacts in CMIP5 simulations. *J Geophys Res* 118:5029–5060.
28. Andrews T, Gregory JM, Webb MJ, Taylor KE (2012) Forcing, feedbacks and climate sensitivity in CMIP5 coupled atmosphere-ocean climate models. *Geophys Res Lett* 39: L09712, 10.1029/2012GL051607.
29. Hasselmann K (1979) On the signal-to-noise problem in atmospheric response studies. *Meteorology of Tropical Oceans*, ed Shaw DB (Royal Meteorological Society, London), pp 251–259.
30. Santer BD, et al. (2011) Separating signal and noise in atmospheric temperature changes: The importance of timescale. *J Geophys Res* 116:D22105, 10.1029/2011JD016263.
31. Schmidt GA, et al. (2012) Climate forcing reconstructions for use in PMIP simulations of the Last Millennium. *Geosci Model Dev* 5:185–191.
32. Gao C, Oman L, Robock A, Stenchikov GL (2007) Atmospheric volcanic loading derived from bipolar ice cores: Accounting for the spatial distribution of volcanic deposition. *J Geophys Res* 112:D09109, 10.1029/2006JD007461.
33. Solomon S, et al. (2010) Contributions of stratospheric water vapor to decadal changes in the rate of global warming. *Science* 327(5970):1219–1223.
34. Solomon S, et al. (2011) The persistently variable "background" stratospheric aerosol layer and global climate change. *Science* 333(6044):866–870.
35. Solomon S, Young PJ, Hassler B (2012) Uncertainties in the evolution of stratospheric ozone and implications for recent temperature changes in the tropical lower stratosphere. *Geophys Res Lett* 39:L17706, 10.1029/2012GL052723.
36. Trenberth KE, Fasullo JT (2010) Simulation of present-day and twenty-first-century energy budgets of the Southern Ocean. *J Clim* 23(2):440–454, 10.1175/2009JCL13152.1.